Accepted Manuscript

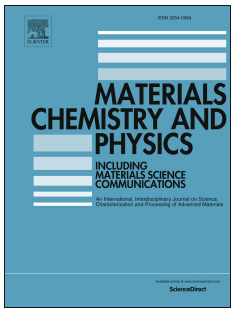

PEO-PPO-PEO surfactant exfoliated graphene cyclodextrin drug carriers for photoresponsive release

Matthew D.J. Quinn, Tao Wang, Mohammad Al Kobaisi, Vincent S.J. Craig, Shannon M. Notley

PII: S0254-0584(17)30882-9

DOI: 10.1016/j.matchemphys.2017.11.012

Reference: MAC 20132

To appear in: *Materials Chemistry and Physics*

Received Date: 9 August 2017

Revised Date: 22 October 2017

Accepted Date: 5 November 2017

Please cite this article as: M.D.J. Quinn, T. Wang, M. Al Kobaisi, V.S.J. Craig, S.M. Notley, PEO-PPO-PEO surfactant exfoliated graphene cyclodextrin drug carriers for photoresponsive release, *Materials Chemistry and Physics* (2017), doi: 10.1016/j.matchemphys.2017.11.012.

PEO-PPO-PEO surfactant exfoliated graphene cyclodextrin drug carriers for photoresponsive release

Matthew D. J. Quinn [a*], *Tao Wang* [b], *Mohammad Al Kobaisi* [c], *Vincent S. J. Craig* [a] *and Shannon M. Notley* [a,]

[a] Department of Applied Mathematics, Research School of Physics and Engineering, The Australian National University, Canberra, 2601, Australia

[b] School of Materials Science and Engineering, Nanchang University, Nanchang, Jiangxi, 330031, China

[c] School of Science, Faculty of Science, Engineering and Technology, Swinburne University of Technology, Hawthorn, Melbourne, 3122, VIC, Australia

KEYWORDS: photothermal, graphene, hydrogel, near-infrared, 2D, drug release

ABSTRACT: Liquid exfoliated graphene sheets were incorporated within α-cyclodextrin-triblock copolymer supramolecular hydrogels prepared with a range of polyethylene oxide and polypropylene oxide block sizes and ratios allowing control over the release properties. The strong photothermal activity of graphene was employed to externally activate drug release from within the gels using near-infrared (NIR) irradiation. These supramolecular hybrid hydrogels

showed thermoreversible changes in viscosity, which is necessary for an injectable, multiple release point drug delivery depot. This hybrid graphene-surfactant-α-CD gel system with thermoreversible properties is demonstrated herein to be externally NIR activated to induce controllable drug release.

Introduction

Graphene has extraordinary thermal, electronic and mechanical properties,[1-4] as well as a strong absorbance in the NIR and a low toxicity, making it a promising nanomaterial for drug release applications.[5-9] There are several well established graphene production methods; (i) physical exfoliation allows high quality sheets to be prepared but at very low yield;[10, 11] (ii) chemical exfoliation can produce large quantities, but the properties are adversely affected;[12, 13] (iii) chemical vapour deposition produces larger sheet sizes but at a higher price and with a lower yield.[14, 15] Alternatively, sonication and shear methods in appropriate solvents or in the presence of surfactant, such as the method employed herein, can produce defect free sheets at high concentrations.[16-18]

Surfactant assisted liquid exfoliation has been demonstrated to produce high quantities of single and few layer pristine graphene sheets as described previously.[18, 19] Pristine graphene exfoliation refers to graphene produced with negligible oxidation or basal plane defects, with only edge defects present in any appreciable concentration.[18] All graphene referred to within this study is considered to be defect free and is referred to as pristine. The surfactant molecules aid in the initial separation of the sheets by minimizing the interfacial tension between the liquid medium and the sheets. By employing large triblock copolymers (Pluronics®) the surfactant molecules also act to prevent reaggregation as the polypropylene oxide (PPO) segments are adsorbed onto

the basal plane and the large polyethylene oxide (PEO) groups extend into solution, sterically preventing suspension collapse.[20]

The addition of the cyclic oligosaccharide molecule α-cyclodextrin (α-CD) into a surfactant exfoliated graphene suspension allows a supramolecular network to be formed with the resulting gel incorporating a homogenous dispersion of graphene.[21, 22] It has been reported by several groups that the α-CD molecule acts as a host molecule and threads onto available PEO groups to form the network, whereby the host-guest interactions occur via non-covalent interactions, such as hydrogen bonding and hydrophobic to hydrophobic interactions.[23-25] As the inclusion complexes are formed, the network extends throughout the medium and large-scale gelation results.[26] The resulting complexes formed are necklace-like supramolecular structures referred to as polypseudorotaxanes.[27]

Supramolecular hydrogels are highly attractive for drug delivery applications due to their thermoreversible nature,[28, 29] their ease of preparation as well as their inherent biocompatibility and biodegradability.[30-32] As such, these hydrogels have been extensively studied for a range of different protein and peptide deliveries.[33-36] Systems have been designed to be pH or temperature sensitive in order to allow a triggered release, whilst providing protection to the payload prior to reaching the targeted site.[37] With such temperature activated systems, the challenges then shift to activating localized heating *in situ*. The use of near-infrared (NIR) light and suitable transducing materials may answer these challenges.

The NIR region extends from approximately 650 to 900 nm and is known to be a suitable range for biological applications as absorption by water and many other biological tissue components in this region is weak, therefore non-specific photothermal heating is minimized.[38] By

incorporating a NIR responsive photothermal agent within the gel, the challenges of externally activating localized heating deep within organic tissue can be addressed.

A number of graphene-based materials have been explored for photothermal applications with varying levels of success.[19, 39, 40] Pristine graphene sheets with no oxidized sites on the basal plane are excellent absorbers of NIR compared to that of the oxidized counterpart graphene oxide (GO), even when this material is subsequently reduced to regain conjugation.[40] The strong absorption of graphene across a broad range of wavelengths combined with the remarkable thermal conductivity of the material, makes it a strong candidate for photothermal applications.[19, 41] Additionally, as the graphene sheets are atomically thin, the surface area to mass ratio is highly suitable for optimal absorption and heat transfer.

For any system considered for *in vivo* applications the biocompatibility of all components is of paramount importance. Several studies have that graphene has low cytotoxicity,[9, 42] which is further reduced in the presence of the highly biocompatible polyethylene glycol (PEG) or non-ionic triblock copolymers,[43-45] enabling significant doses of graphene to be safely employed. When the inherent biocompatibility is considered in conjunction with the excellent photothermal ability of graphene nanosheets, the use of a thermoreversible drug delivery depot loaded with photoresponsive graphene appears to be a highly promising system. Here, the effectiveness of graphene nanosheets as NIR thermoresponsive agents for the promotion of triggered release is investigated.

Materials and methods

Graphene suspension preparation and characterization

Natural graphite flakes, α-CD and four triblock copolymers; F108, F68, L64 and P123 were purchased from Sigma Aldrich and used in this study without further purification (see Table S1 for specifications).

To produce graphene, suspensions of graphite flakes and surfactant were prepared at 0.5 wt.% and 0.1 wt.% respectively. Graphite suspensions in batches of 200 ml were maintained at 25 °C via a cooling jacket while ultrasonicated with a Q700 Qsonica ultrasonicator and a 13 mm flat head probe with replaceable tip at an amplitude of 40 % for 2 hours. Resulting suspensions were then centrifuged at 3000 relative centrifugal force (*rcf*) for 10 minutes.

The extent of exfoliation was monitored using UV-visible spectroscopy. The concentration of graphene in suspension at sequential stages of sonication was determined using a UV-1800 Shimadzu UV Spectrophotometer via the absorbance at 750 nm using the extinction coefficient 4237 ml mg^{-1} m^{-1} determined by Paton et al. (Figure 1a).[46] The absorbance spectra for the graphene materials was also measured using a UV-310PC Shimadzu UV-vis-NIR spectrometer. The absorbance spectra of GO and reduced graphene oxide (rGO), purchased from Graphenea, were measured to provide a comparison against the pristine graphene produced and used within this study (Table S2). Each suspension was then adjusted to 0.03 mg ml^{-1} for all further experiments or characterization tests unless otherwise stated. The graphene produced was also characterized using Raman spectroscopy, utilizing a Renishaw Raman inVia Reflex with a laser excitation of 532 nm. The particles were added dropwise to a 0.22 µm pore size alumina filter (Whatman) to 500 µL and spectra were collected with a 100 x lens with a 2400 l/mm grating (Figure 1b).

A Jeol 2100F transmission electron microscope (TEM) was used to image graphene sheets throughout the study (Figure 1c). The nanosheets were deposited onto holey carbon TEM grids

by vacuum suctioning 100 µL of 0.03 mg ml^{-1} suspension and allowing the samples to dry for 24 hours.

Scanning electron microscopy (SEM) images of the exfoliated graphene sheets were collected to contribute to general morphology and exfoliation elucidation using a Zeiss UltraPlus FESEM without any coating at a voltage of 1 kV. Samples were added dropwise to an Alumina filter as per the Raman sample preparation.

A Multimode 8 AFM (Bruker) atomic force microscope (AFM) was used to image graphene samples using ScanAsyst-Air mode. Bruker ScanAsyst-Air probes with nominal tip radii of 2–12 nm and a silicon nitride cantilever of spring constant, 0.4 N m^{-1} were employed. Analysis on flattened images was conducted using NanoScope Analysis software (V 1.5, Bruker) (Figure 1d and 1e). Samples were prepared on silicon wafer as described by Wang et al. in 2017.[47]

The NIR photothermal properties of the neat graphene suspensions was investigated by performing a concentration series of photothermal heating curves. A 0.5 ml aliquot was transferred into a 4 ml glass cuvette (cut down to hold a maximum of 2 ml) and fitted into an insulated cuvette holder inside a light box. An 808 nm laser diode was positioned outside of the light box (to avoid an additional heat source) with an optic fibre positioned within the light box directed at the cuvette. A convex lens was used to focus the beam in the middle (both face and depth) of the cuvette. The 808 nm 500 mW laser with a spot size of 1.7 mm was then turned on and the temperature measured for 15 minutes. Samples were mixed throughout the experiment using a magnetic stirrer bar to ensure even heat distribution. It is important to note that the laser geometry, suspension volume and concentration will influence the temperature changes observed. Some slight fluctuations in the observed photothermal curve maximums are attributed to room temperature variations.

α-CD gel preparation and characterization

Solutions of α-CD and surfactant were prepared and mixed to give a final α-CD concentration of 100 mg ml^{-1} and 2 wt.% of surfactant unless otherwise stated.

To study the gelation process a Rheometrics Dynamic Stress Rheometer (DSR) with 25 mm diameter parallel plates was used. Dynamic time sweep measurements at 10 rad s^{-1} frequency and 10 Pa stress at 25 °C were conducted. These conditions were selected to ensure that the yield point of any of the gels was not exceeded.

All gels were freeze-dried prior to imaging, the dry gel was then transferred onto the SEM stage and mounted with electrically conductive tape. SEM images were performed using a Zeiss UltraPlus FESEM with gel samples coated with platinum at 10 mA for 2 minutes prior to imaging at a voltage of 1 kV.

α-CD gel drug release parameters

A typical gel sample was composed of 2 wt.% surfactant, 0.03 mg ml^{-1} graphene suspension and 1 mg ml^{-1} fluorescein as the drug model and is referred to here as α-CD-*surfactant*-graphene. Gel components were mixed in 5 ml glass rounded 10 mm diameter cuvette tubes 75 mm in height to a total volume of 1 ml of gel with α-CD at a concentration of 100 mg ml^{-1}. The fluorescein was loaded into the α-CD solution and the pH was adjusted to 9.5 with sodium hydroxide, to allow the fluorescein to fully dissolve. All components (excepting the nanosheets) were dissolved prior to mixing. Immediately following mixing, the mixture was sonicated for 10 seconds, then covered with parafilm to avoid moisture loss and allowed to stand for approximately 6 hours. The control samples were prepared both with and without graphene. To remove any fluorescein from the walls of the vial, 6 hours after preparation, 4 ml of phosphate buffer solution (PBS) was added on top of the gel and left to stand for 16 hours prior to the release test. Immediately prior

to the release test the PBS was discarded, the vial rinsed 3 times with PBS and a fresh 4 ml aliquot of PBS was added to the vial. The sample to be irradiated was then placed in the path of the 808 nm, 500 mW beam and the control samples were placed inside the light box approximately 30 cm away from the primary sample. The temperature within the light box was measured in both sample positions to ensure all samples experienced an even ambient temperature throughout the experiment. The laser was then turned on for the required period and then switched off before sample extraction. Each sample had the aqueous phase mixed prior to a 750 µL aliquot being taken, after which 750 µL of fresh PBS was added to the vial and the samples returned to the light box. Fixed extraction times (laser off times) were maintained at 4 minutes throughout all experiments.

The aliquot was then centrifuged for 2 minutes at 4000 *rcf* to remove any graphene that had migrated into the PBS layer and then 500 µL was taken and the absorbance was measured at 490 nm. All release experiments were performed at room temperature which was monitored during all experiments and shown to be 22.0 °C ± 1.5 °C. An additional confirmatory experiment was performed using a lower power (75 mW) 785 nm laser diode at 37 °C.

Results and discussion

Graphene production

The characteristic absorbance scan for exfoliated pristine graphene shows the peak maximum at 270 nm indicative of non-oxidized graphene sheets.[48] The wavelength scan also shows a strong and broad absorbance in the infrared region that is stronger than GO and reduced graphene oxide (rGO) (Figure 1a). The trend of the strengthening NIR absorbance with increasing conjugation is

particularly clear when an incompletely reduced GO sample is compared, showing a strong increase in absorbance between that of GO and fully reduced GO (Table 1).[40]

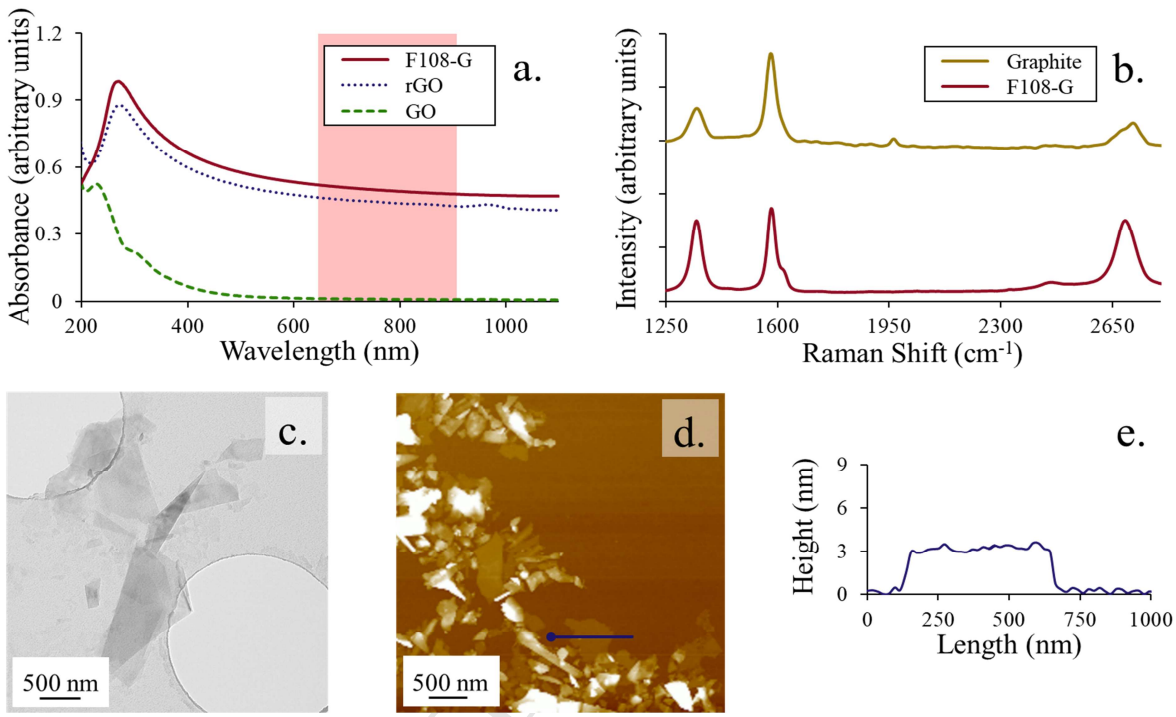

Figure 1. (a.) UV-visible absorbance spectra of the initial F108-graphene suspension (solid red line), GO (green long dashes) and rGO (blue dots), with the NIR region highlighted (pale red box) and all samples at matched concentrations of 0.01 mg ml^{-1}. **(b.)** Raman spectra showing unexfoliated graphite (top) and exfoliated F108-graphene (bottom) clearly showing the shoulder on the 2D peak only present for the unexfoliated graphite. **(c.)** A TEM image of F108-graphene suspension nanosheets. **(d.)** An AFM scan of the F108-graphene nanosheets with a **(e.)** marked cross section.

Table 1. Extinction coefficient and absorbance at 808 nm for each graphene type material.

Extinction coefficient (ml mg^{-1} m^{-1})	Absorbance at 808 nm (fixed 1 mg ml^{-1})
4237 $_{@750\ nm}$[46]	47.73
7380 $_{@\ 265\ nm}$[40]	36.68
7380 $_{@\ 265\ nm}$[40]	28.00[40]
6150 $_{@\ 230\ nm}$[40]	6.08

The Raman spectra collected provides thickness information through the ratio of the intensity of the G and 2D peaks, I_{2D}/I_G, which is 1:0.87 for the presented spectrum, indicating highly exfoliated graphene sheets.[49, 50] The shape and positioning of the 2D peak indicates a highly exfoliated sample approaching that of monolayer graphene (See Figure S3). The D peak is expected to be present for the Raman spectra collected for sheets of this size as the laser diameter is larger (0.87 µm) than the sheets and will therefore detect the sp^3 hybridized carbon atoms of the sheet edges.[16] The full width half maximum (FWHM) for the 2D peak is 70 cm^{-1} which indicates this is likely a bi-layer spectrum.[51]

The size distribution of the graphene sheets was determined via dynamic light scattering (DLS) showing average hydrodynamic diameters of 370, 195 and 310 nm for materials exfoliated using F108, F68 and L64 respectively which follow previous reports (Figure S1).[52, 53] In addition to the DLS measurements, a number of image analysis methods including TEM, AFM and scanning electron microscopy (SEM) were used to fully characterize the sheets (see Figure S2 for SEM).

The AFM scan gives definitive sizing information shown through the cross-sectional thickness of the sheet marked in Figure 1d. However, the graphene sheets likely have a surfactant and water coating present, increasing the observed thickness.[47, 49] Additionally, ensuring the sheets are deposited flat on the silicon wafer substrate is challenging as sheet folding and stacking contribute to convoluted scans. The polydispersity of the single and few layer graphene sheets can also be observed in the AFM scans.

In addition to the sizing and thickness analysis, we have demonstrated the structural integrity of the graphene through TEM electron diffraction (Figure S11).

Photothermal properties of pristine graphene

Single and few layered graphene sheets produced via liquid exfoliation are suitable photothermal agents due to the strong and broad absorbance in the NIR region. As can be seen in Figure 1a, the absorbance of pristine graphene sheets is far stronger in the NIR region than that of both GO and rGO indicating substantially better photothermal efficiency. It is clear that the surfactant assisted liquid exfoliation production method is far more suited than the chemical exfoliation approaches towards preparing a photothermal agent for such roles.

The photothermal properties of the graphene suspensions were characterized via simple photothermal heating curves, as shown in Figure 2., using a wavelength in the center of the NIR region. The stability of these suspensions under ambient and elevated temperatures is also without competition, with many similar photothermal materials showing a decrease in efficiency after several cycles,[54, 55] as has been demonstrated previously.[19]

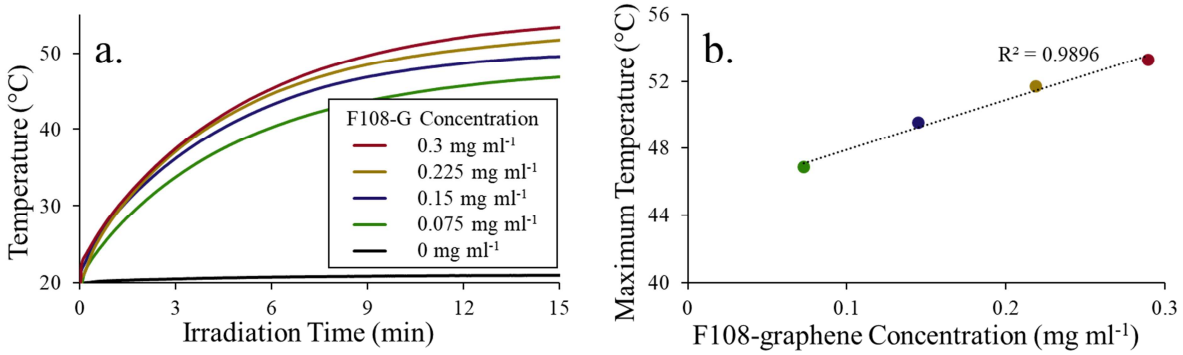

Figure 2. (a.) Photothermal curves as function of concentration showing in ascending order; 0, 0.075, 0.15, 0.225 and 0.30 mg ml^{-1} F108-graphene over 15 minutes of irradiation. **(b.)** The respective temperatures achieved after 15 minutes as a function of graphene concentration.

For photothermal applications, high thermal conductivity (reported as high as 5000 W m^{-1} K^{-1})[56] is important for dissipating the localized heat within the system. For single and few layer graphene the thermal conductivity at room temperature is primarily dictated by acoustic phonons. As there is a clear change in the behavior of the Raman active phonons, as indicated by Figure 1b, it can be assumed that the acoustic phonons and therefore the thermal properties of the exfoliated graphene sheets have been altered and improved.[3] Further, as the production method does not produce defects within the basal plane,[57] the phonon scattering at such points is minimized, maintaining the desired thermal properties. The extent of the contribution of internal thermal properties on the external heat dissipation within the system remains unclear with significant barriers requiring consideration such as the Kapitza resitance.[58-60] However, percolation events[61, 62] and Ballistic transfer linking[63, 64] will likely result to allow substantial improvements on the bulk thermal transfer.[65]

Photothermal release

α-CD-surfactant drug release studies

The unstimulated release profiles for each of the three surfactant systems F108, F68 and L64 demonstrates that the different compositions produce subtly different gels which influence the release rates of the drug model significantly (Figure 3a). The F108 and F68 surfactant based gels, both with an 80 wt.% PEO composition but with substantially different sizes (14600 and 8400 Da respectively), showed very similar release profiles, indicating that the size difference between these surfactants has a minimal effect on the final product. The release rates of the two high PEO composition surfactants showed a significant decrease when compared to that of the smaller surfactant with the lower PEO composition, L64 (2900 Da).

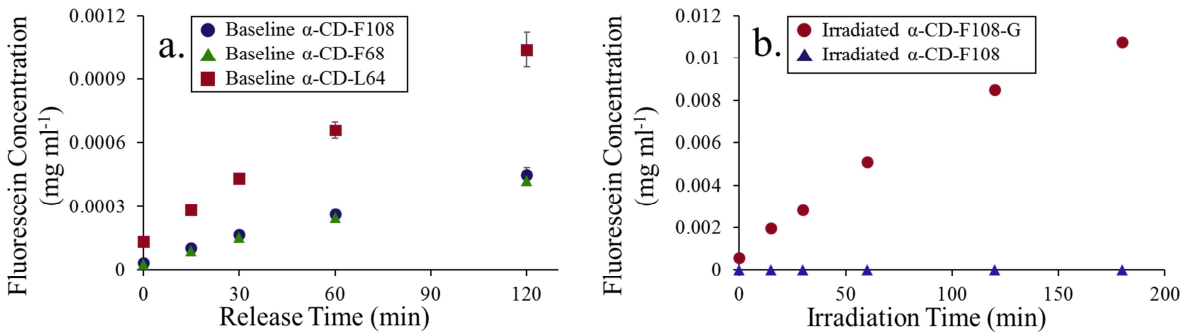

Figure 3. (a.) Baseline release for each α-CD-surfactant showing the different release rates for F108 (blue circles), F68 (green triangles) and L64 (red squares). Error bars show the maximum and minimums and the data presented is the average of three samples. **(b.)** Concentration of fluorescein released from irradiated α-CD-F108-graphene gel (red series) and irradiated α-CD-F108 gel (blue triangles) demonstrating the photothermally induced drug release. To show the photothermally induced release the blank release values are subtracted from both series.

The larger release rate of the L64 based gel reflects a more open internal network that allows the fluorescein molecules (1.09 nm maximum length[66]) to discharge. The irradiated α-CD-F108-graphene gel showed a dramatic increase in the concentration of fluorescein released into the PBS compared to that of the stimulated graphene free gel (Figure 3b). As such the blank sample data (sample with no graphene present) was subtracted from that of the graphene loaded sample to easily observe the stimulated release values. This demonstrated that no component of the α-CD-surfactant system (other than the photothermal agent) was absorbing sufficient amounts of the NIR light to induce any additional drug release. There was no identifiable difference in the unstimulated release rates of the graphene loaded gel or that of the irradiated un-loaded graphene gel (Figure S4). It is a fair assumption that the drug model fluorescein could interact with graphene in the gel through π-π stacking, however as no changes were observed between graphene loaded and graphene free unstimulated gel samples, if this event is occurring it is of a

negligible extent and effect. Further, it is likely that the surfactant previously adsorbed during the exfoliation process will leave little room for significant graphene to fluorescein interaction.

The irradiation profile of the α-CD-F108-graphene gel versus that of the unloaded counterpart indicates that the increase in fluorescein release was entirely due to the photothermal action of the graphene sheets, resulting in localized heating. This localized heating was likely expanding the gel network or simply inducing enough of a phase change to activate the increased diffusion of fluorescein. Further, it has been demonstrated previously that hydrogen bonding plays a significant role in the interaction between PEO and α-CD moieties.[25, 67] Therefore it is fair to assume that as the hydrogen bonding is disrupted by the localized high temperature conditions upon irradiation and that the inclusion complexes are weakened inducing gel expansion and breakdown with a corresponding spike in fluorescein release.[25, 68]

The thermoreversible nature of the prepared gels allowed an activation switch cycle to be demonstrated by simply alternating periods of irradiation and non-irradiation sequentially, and measuring the fluorescein release (Figure 4a). The release of fluorescein during the photothermally activated periods presented a marked increase, while the non-irradiated sample showed a consistent low rate of release. The release rates between the activated and non-activated periods could then be directly compared by looking at the ratio of the fluorescein concentration released during each segment for the sample and blank (Figure 4b). This showed a marked difference between the release rates and also showed a slow upwards trend, likely indicating a decrease in the integrity of the gel structure with multiple heating and cooling cycles, or a slight residual increase in baseline temperature.

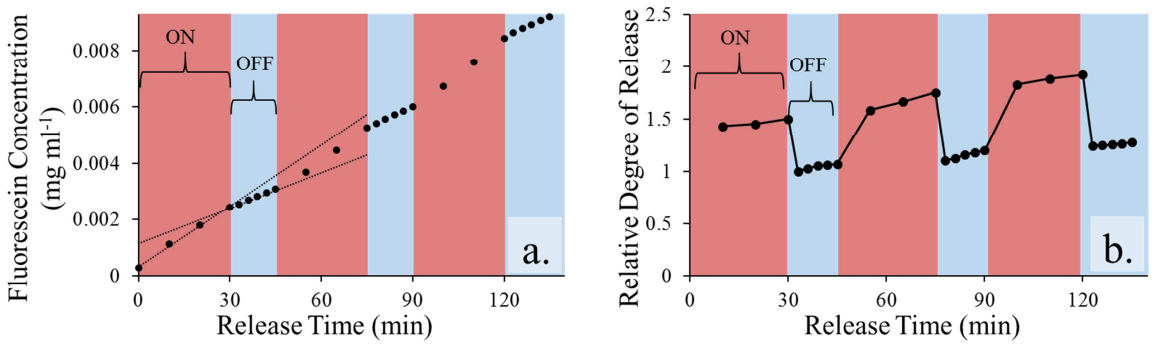

Figure 4. (a.) α-CD-F108-graphene gel photothermally induced drug release with alternating laser on off periods to demonstrate the reversible nature of the gel. **(b.)** The relative degree of release of the irradiated graphene loaded gel and the release rate of the control.

In order to demonstrate the versatility of graphene in the role of photothermal drug release activator a confirmatory experiment was performed using a laser with a different wavelength of 785 nm (Figure S9). The same trend was observed showing the flexibility provided by the strong, broadband absorbance of the graphene sheets. This is of particular value as one of the limitations observed for gold nanoparticles is the specificity of wavelengths required for activation, a challenge circumvented by a broadly absorbing material. This again reinforces the suitability of graphene in this role.

From the fluorescein drug release experiments a clear correlation between the surfactant molecular architecture (likely due to the PEO compositions) and the observed release rates is demonstrated (Figure 3a.). In an attempt to understand the observed differences in release profiles the gel viscoelastic properties were explored.

Influence of surfactant composition on gel properties

The gelation kinetics of α-CD with F108, F68, L64, and P123 surfactants were explored in this study (see Table S1 for compositions). The evolution of storage (G') and the loss moduli (G'') were measured in time sweep experiments immediately after mixing the gel components (Figure 5). The G' and G" increase as the α-CD molecules thread onto the PEO chains. The point at which the elasticity modulus crosses over the loss modulus is the gel point, a property characteristic of viscoelastic gel materials.

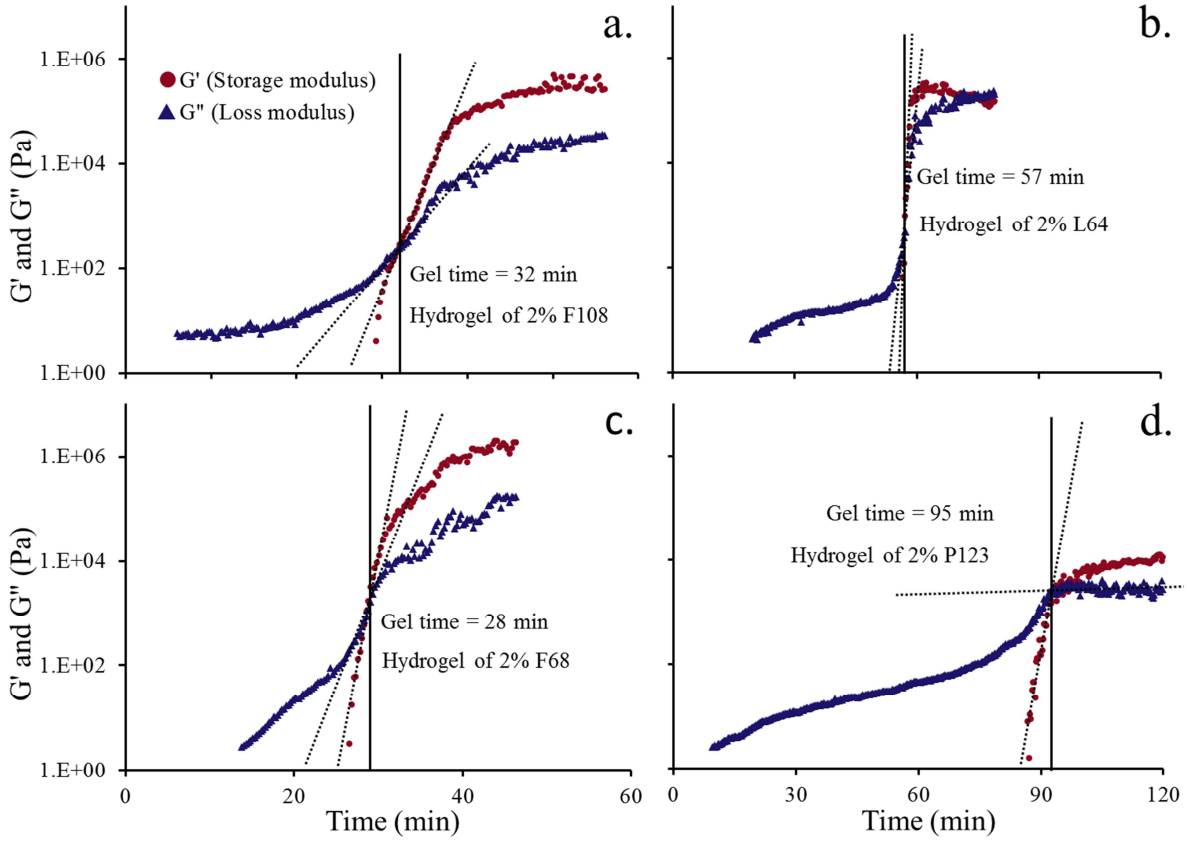

Figure 5. Gelation kinetics of the α-CD gels formed with 2% of **(a.)** F108, **(b.)** L64, **(c.)** F68 and **(d.)** P123, measured by the evolution of the storage (G') (red circles) and loss (G'') (blue triangles) moduli in time sweep experiments at 25 °C.

The gel point of the α-CD based gels shows a clear dependency on the surfactant chemical structure, specifically the PEO ratio in their molecular structure (See Figure 6). For the F108 system, a large triblock copolymer (14600 Da) with a PEO composition of 80 wt.%, the PEO groups are readily available for α-CD threading, resulting in a short gel point time. Compared to that of the L64 system, a 40 wt.% PEO composition surfactant (2900 Da), the gel time is considerably larger than that of the F108 system. This emerging trend is clearly demonstrated when comparing both the F108 and F68 (80 wt.% PEO, 8400 Da) based gels to the L64 and then to the P123 (30 wt.% PEO, 5750 Da) based gels showing that with decreasing PEO composition, gel formation is slowed. It is also likely that the critical micelle concentration (CMC) values, which at 2 wt.% are exceeded for the L64 and P123 surfactants, may be slowing the gel formation time as the micelles must be broken before the PEO chains are available to partake in the gel formation (Table S1 for CMC values).

The co-assembly of the α-CD and PEO moiety of the surfactants in the gelation process is dependent on the geometry of these two components. The cross-section diameter of a PEO unit is 3.1 Å,[27] and the diameter of the α-CD cavity is 4.7 Å,[27] providing matching geometries to allow the PEO chain to thread into the α-CD rings. As the height of the α-CD cavity (7.9 Å) is approximately twice the contour length of the PEO repeat unit, multiple α-CD molecules can thread onto the polymeric surfactant chains.[27] As the surfactant with the shorter PEO chains (F68) based gels showed no significant difference in the gel point time to that of the surfactant with the longer PEO chains (F108), it appears that even this significant difference in surfactant size does not influence the efficiency of the PEO to α-CD interaction.

The gel point for each surfactant system was also explored using a simple “inversion test” where the gels were considered formed when no visible movement could be observed for 30 seconds

when placed upside down (Figure S5).[69] The results correlated well with the rheologically determined gel points, but the inversion test experiment does have a bias, inferring a delayed end point as it relies on the viscosity being sufficient to stop the movement of the entire gel matrix, which may occur well after the cross over point of the storage and loss moduli. Additionally, the inversion test highlighted that the α-CD-P123 gels did not form a gel of sufficient stability to be used for the release assays and was therefore not further explored. This is supported by the maximum measured storage modulus (Table 2) for the P123 system which was considerably lower than the other gels exhibited. The F68 system showed the greatest overall increase in maximum storage modulus which is likely due to the high PEO content, in addition to the smaller size of the polymers, forming a strongly connected but brittle gel.[70]

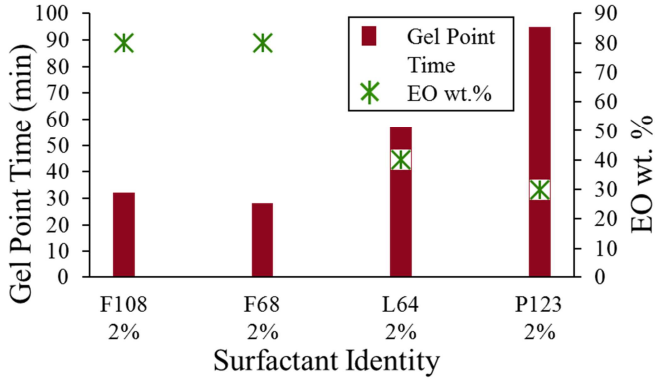

Figure 6. Average gelling points *(G'/G'' Crossover point)* as a function of different surfactant (red bars) and the PEO wt.% for each surfactant (green asteriks).

Table 2. The gel point times and the maximum storage modulus (G)' for respective surfactant based gels.

Surfactant	Gel point (min)	Maximum G' (kPa)
F108	32	206
F68	28	828
L64	57	268
P123	95	16

A concentration series of F108 based α-CD gels were prepared to further explore the gelling mechanism of these systems. This again demonstrated the relationship between increased PEO concentration and that of the faster gelling time (Figure 7a). The full viscoelastic plots can be seen in Figure S6. These results follow similar trends previously reported in literature whereby gelling time and release rates are faster with the increased concentration of cross-linker, or in this case the inclusion complex components (α-CD).[21, 27, 30] In addition to studying the influence of surfactant concentration, a graphene concentration series was established which showed a distinct delay in the gel formation upon the addition of graphene. This was evident with even the lowest graphene concentration explored. Both the graphene present and graphene free samples showed a strong linear dependence on the surfactant concentration. No further change in the gelling time with increasing graphene concentration was observed (Figure 7b). As the α-CD molecules are much smaller than all other components within this system, they would likely be the most mobile group and therefore the gelation mechanism should be viewed as the α-CD molecules threading onto the PEO chains, as opposed to the PEO chains entering the cavity of the α-CD molecules. This graphene concentration series indicates that the initial concentration of nanosheets was sufficient to sterically inhibit the mobility of the α-CD molecules within the solution whilst the large-scale network is forming. This is reasonable as the graphene sheets are by far the least mobile component within the gel matrix due to size and geometry. The full

viscoelastic plots of the graphene loaded gels as a function of surfactant concentration can be seen in Figure 7c.

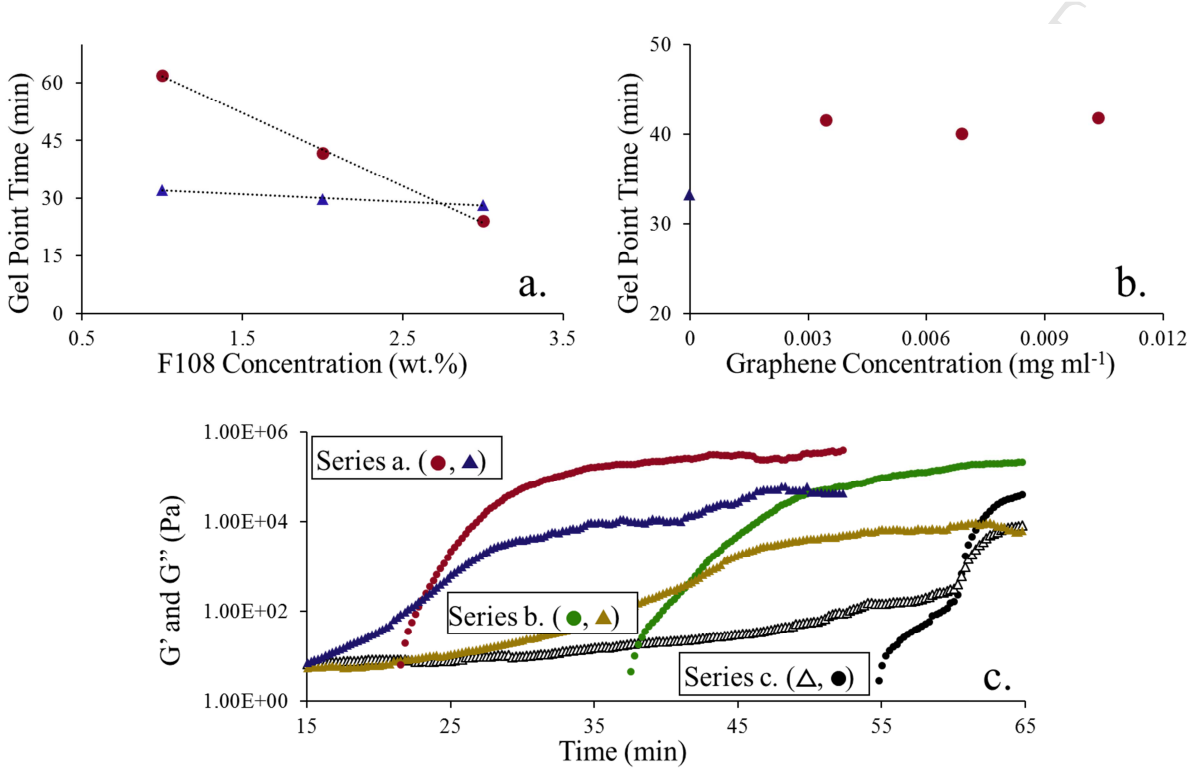

Figure 7. (a.) Average α-CD-F108 gel point as a function of F108 concentration with (blue triangles) and without (red circles) graphene (0.03 mg ml^{-1}). **(b.)** The gel point as a function of graphene concentration at a fixed F108 concentration of 2 wt.%, showing a distinct delay in gel formation time and then negligible further change with increasing graphene concentration. **(c.)** Time sweep data for 0.03 mg ml^{-1} graphene loaded gel with F108 concentrations of 3 **(series a.)**, 2 **(series b.)** and 1 **(series c.)** wt.%.

SEM images were used to study the morphology and micro-structure of the gels explored within this study. The SEM images show the porous three-dimensional network of the dried α-CD gels,

giving an approximate indication of pore sizes within the network, however possible artifacts associated with the freeze-drying process must not be ignored (see Figure 8).

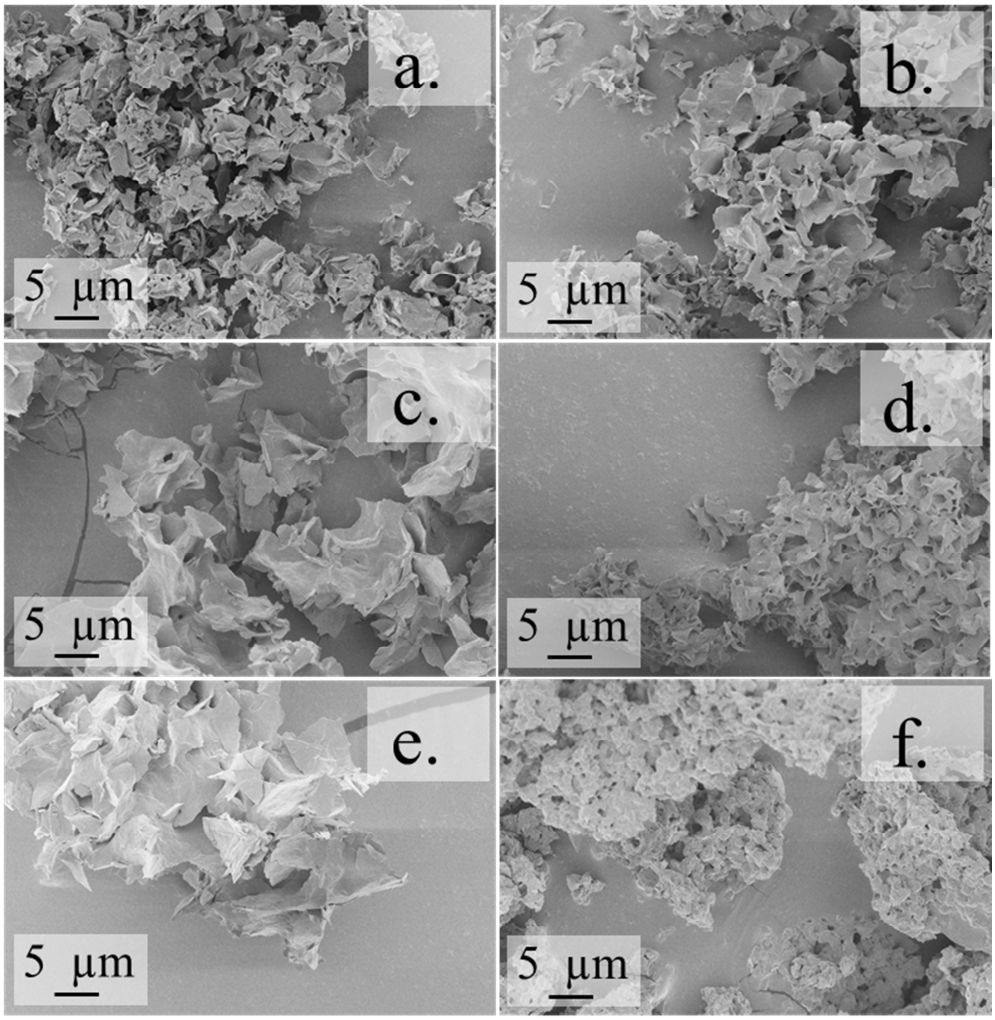

Figure 8. SEM images of freeze-dried α-CD gels with **(a.)** F108-graphene, **(b.)** F108, **(c.)** 4% F108, **(d.)** F68, **(e.)** L64 and **(f.)** P123 at 5,000 x magnification. All gels were prepared at 2 wt.% respective surfactant concentration unless otherwise stated.

The crystals of the α-CD gels appear as lamellar flakes with well-defined edges in the majority of the freeze-dried samples as described previously.[27] Several morphological variations can be

observed when the SEM images of the different surfactant based α-CD systems are compared, the presence of graphene, however, does not appear to present an identifiable change similar to previous reports (Figure 8a and 8b).[21] The lamellar flakes forming for the neat 2% F108 gel (Figure 8b) appear slightly smaller and less connected than those of the 4% F108 gel (Figure 8c). Interestingly the L64 gel (Figure 8e) shows a larger and less dense network than the F108 and F68 based gels, which could potentially be linked to the increased release rate (Figure 3a). The P123 gel appears to be a highly dense structure with much smaller pore sizes (Figure 8f). The morphologies of both the 2% F108 (Figure 8b) and F68 gels (Figure 8d), both with a PEO wt.% of 80, do not appear significantly different, which correlates strongly with the almost identical release rates observed for each.

In a further attempt to gain insight into the microstructure of the α-CD gels, XRD scans were performed for each of the surfactant type gels as well as the neat α-CD powder (Figure S10). The XRD spectra of the freeze-dried gels show the characteristic strong peak at approximately 2θ = 20.0° (d = 4.44 Å) which is assigned as the 210 reflection.[29, 67] The channel-type crystalline structure resulting from the long-chain nature of the guest-molecules (PEO segments) has been well studied and the corresponding peaks have been identified in both hydrated and freeze-dried gels.[29] The 210 reflection can be observed as a sharper, more well defined peak for the 4% F108 α-CD gel present at 2θ = 19.905 while the F108 and L64 surfactant gel shows a broader peak at a slightly lower diffraction angle of 2θ = 19.795. The broader peak indicated a less crystalline structure with lower surfactant compositions.

The thermoreversible nature of these α-CD gels determined previously,[23] was explored to demonstrate the injectability of this drug delivery depot preloaded with both the photothermal and medically active agent (Figure 9). A substantial decrease in viscosity was observed to occur

below or near the cloud point of the employed surfactants respectively suggesting that a sufficient phase change had occurred and the α-CD molecules were disassociating from the PEO segments. The gel system reformed after a short period of time post excitation, demonstrating the recovery of the complex. The ability of the gels to reform the stable complex after heating is particularly important for a potential drug depot application allowing spikes of drug release to be controlled.

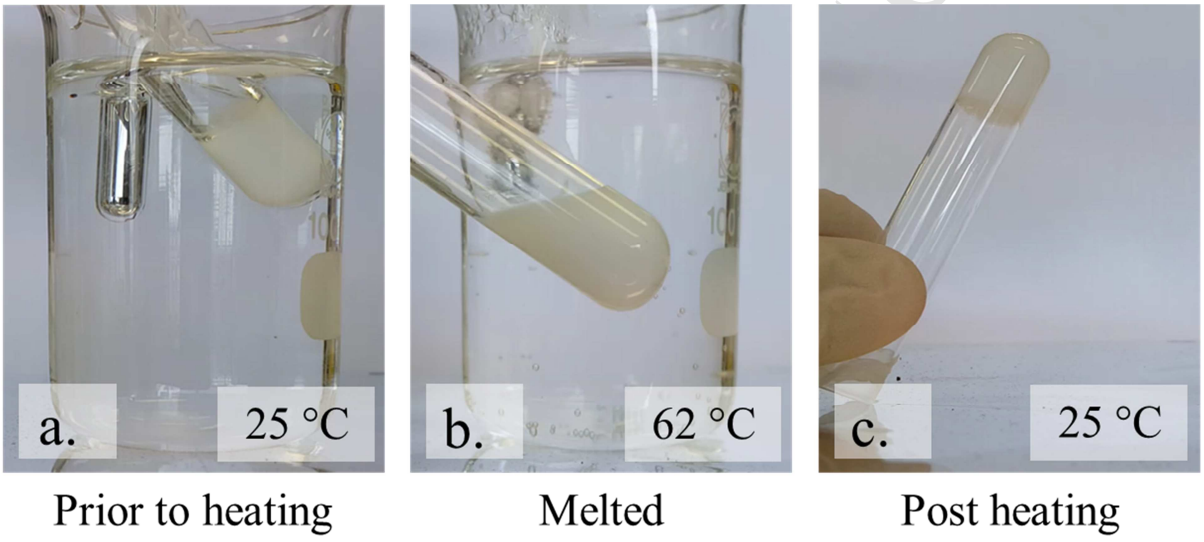

Figure 9. Images of an α-CD-L64 based gel demonstrating the thermoreversible nature of these systems with the gel **(a.)** prior to heating, **(b.)** immediately after heating and **(c.)** 5 minutes after heating.

The gel studies showed a strong correlation of gel formation time with that of the PEO composition of the surfactant and with the observed release of fluorescein from the photothermally stimulated gels. As the gel formation time and the PEO composition will influence the packing structure of the final gel product, it is a fair correlation to draw on while not entirely elucidating the mechanism behind the release profile changes.

Conclusion

A range of triblock copolymer surfactants with varying PEO compositions were explored for the formation of a pristine graphene hybrid α-CD gel. The graphene was then externally activated through NIR irradiation resulting in highly localized heating sufficient to activate the release of a drug model from within the gel network. Control by photothermal activation was then demonstrated through a switching experiment showing distinct changes in the relative release rates of the drug model. The thermoreversible nature of the gels and the ability to externally activate release demonstrates that pristine graphene-α-CD hybrid gels are a versatile injectable delivery depot.

ASSOCIATED CONTENT

Supporting Information.

Additional materials and experimental details including further graphene and gel characterization data including full scan rheology measurements, can be found in the supporting information.

The following files are available free of charge.
Figures S1 – S10 and Tables S1- S2 (PDF)

AUTHOR INFORMATION

Corresponding Author

* Matthew D. J. Quinn, E-mail: matthew.quinn@anu.edu.au

Author Contributions

The manuscript was written through contributions of all authors. All authors have given approval to the final version of the manuscript.

ACKNOWLEDGMENT

S.M.N. acknowledge financial support under the ARC Future Fellowship scheme. We thank Dr. Khu Vu (RSPE, ANU) for his valuable advice and the use of his laboratory.

ABBREVIATIONS

α-CD, α-cyclodextrin; α-CD-Pluronic-graphene, α-cyclodextrin-Pluronic-graphene; 2D, two dimensional; TEM, transmission electron microscopy; SEM, scanning electron microscopy; AFM, atomic force microscopy; DLS, dynamic light scattering; NIR, near-infrared; PEO, polyethylene oxide; PPO, polypropylene oxide; *rcf*, relative centrifugal force; PSD, particle size distribution; FESEM, field emission scanning electron microscopy; nm, nanometer; Da, Dalton.

REFERENCES

1. Geim, A. K.; Novoselov, K. S., The Rise of Graphene. *Nat. Mater.* **2007,** *6* (3), 183-191.
2. Castro Neto, A. H.; Guinea, F.; Peres, N. M. R.; Novoselov, K. S.; Geim, A. K., The Electronic Properties of Graphene. *Rev. Mod. Phys.* **2009,** *81* (1), 109-162.
3. Shahil, K. M. F.; Balandin, A. A., Thermal Properties of Graphene and Multilayer Graphene: Applications in Thermal Interface Materials. *Solid State Commun.* **2012,** *152* (15), 1331-1340.
4. Lee, C.; Wei, X.; Kysar, J. W.; Hone, J., Measurement of the Elastic Properties and Intrinsic Strength of Monolayer Graphene. *Science* **2008,** *321* (5887), 385-388.
5. Hu, S. H.; Fang, R. H.; Chen, Y. W.; Liao, B. J.; Chen, I. W.; Chen, S. Y., Photoresponsive Protein-Graphene-Protein Hybrid Capsules with Dual Targeted Heat-Triggered Drug Delivery Approach for Enhanced Tumor Therapy. *Adv. Funct. Mater.* **2014,** *24* (26), 4144-4155.
6. Tian, B.; Wang, C.; Zhang, S.; Feng, L.; Liu, Z., Photothermally Enhanced Photodynamic Therapy Delivered by Nano-Graphene Oxide. *ACS Nano* **2011,** *5* (9), 7000-7009.
7. Yang, K.; Zhang, S.; Zhang, G.; Sun, X.; Lee, S. T.; Liu, Z., Graphene in Mice: Ultrahigh in Vivo Tumor Uptake and Efficient Photothermal Therapy. *Nano Lett.* **2010,** *10* (9), 3318-3323.
8. Quinn, M. D. J.; Wang, T.; Du, J. D.; Boyd, B. J.; Hawley, A.; Notley, S. M., Graphene as a Photothermal Actuator for Control of Lipid Mesophase Structure. *Nanoscale* **2017**.

9. Chen, H.; Müller, M. B.; Gilmore, K. J.; Wallace, G. G.; Li, D., Mechanically Strong, Electrically Conductive, and Biocompatible Graphene Paper. *Adv. Mater.* **2008,** *20* (18), 3557-3561.
10. Novoselov, K. S.; Geim, A. K.; Morozov, S. V.; Jiang, D.; Zhang, Y.; Dubonos, S. V.; Grigorieva, I. V.; Firsov, A. A., Electric Field in Atomically Thin Carbon Films. *Science* **2004,** *306* (5696), 666-669.
11. Novoselov, K. S.; Jiang, D.; Schedin, F.; Booth, T. J.; Khotkevich, V. V.; Morozov, S. V.; Geim, A. K., Two-Dimensional Atomic Crystals. *Proc. Natl. Acad. Sci. U. S. A.* **2005,** *102* (30), 10451-10453.
12. Li, D.; Müller, M. B.; Gilje, S.; Kaner, R. B.; Wallace, G. G., Processable Aqueous Dispersions of Graphene Nanosheets. *Nat. Nanotechnol.* **2008,** *3* (2), 101-105.
13. Eda, G.; Fanchini, G.; Chhowalla, M., Large-Area Ultrathin Films of Reduced Graphene Oxide as a Transparent and Flexible Electronic Material. *Nat. Nanotechnol.* **2008,** *3* (5), 270-274.
14. Kim, K. S.; Zhao, Y.; Jang, H.; Lee, S. Y.; Kim, J. M.; Kim, K. S.; Ahn, J. H.; Kim, P.; Choi, J. Y.; Hong, B. H., Large-Scale Pattern Growth of Graphene Films for Stretchable Transparent Electrodes. *Nature* **2009,** *457* (7230), 706-710.
15. Novoselov, K. S.; Fal'Ko, V. I.; Colombo, L.; Gellert, P. R.; Schwab, M. G.; Kim, K., A Roadmap for Graphene. *Nature* **2012,** *490* (7419), 192-200.
16. Hernandez, Y.; Nicolosi, V.; Lotya, M.; Blighe, F. M.; Sun, Z.; De, S.; McGovern, I. T.; Holland, B.; Byrne, M.; Gun'ko, Y. K.; Boland, J. J.; Niraj, P.; Duesberg, G.; Krishnamurthy, S.; Goodhue, R.; Hutchison, J.; Scardaci, V.; Ferrari, A. C.; Coleman, J. N., High-Yield Production of Graphene by Liquid-Phase Exfoliation of Graphite. *Nat. Nanotechnol.* **2008,** *3* (9), 563-568.
17. Lotya, M.; Hernandez, Y.; King, P. J.; Smith, R. J.; Nicolosi, V.; Karlsson, L. S.; Blighe, F. M.; De, S.; Wang, Z.; McGovern, I. T.; Duesberg, G. S.; Coleman, J. N., Liquid Phase Production of Graphene by Exfoliation of Graphite in Surfactant/Water Solutions. *J. Am. Chem. Soc.* **2009,** *131* (10), 3611-3620.
18. Notley, S. M., Highly Concentrated Aqueous Suspensions of Graphene through Ultrasonic Exfoliation with Continuous Surfactant Addition. *Langmuir* **2012,** *28* (40), 14110-14113.
19. Quinn, M. D. J.; Vu, K.; Madden, S.; Notley, S. M., Photothermal Breaking of Emulsions Stabilized with Graphene. *ACS Appl. Mater. Interfaces* **2016,** *8* (16), 10609-10616.
20. Guardia, L.; Fernández-Merino, M. J.; Paredes, J. I.; Solís-Fernández, P.; Villar-Rodil, S.; Martínez-Alonso, A.; Tascón, J. M. D., High-Throughput Production of Pristine Graphene in an Aqueous Dispersion Assisted by Non-Ionic Surfactants. *Carbon* **2011,** *49* (5), 1653-1662.
21. Zu, S. Z.; Han, B. H., Aqueous Dispersion of Graphene Sheets Stabilized by Pluronic Copolymers:Formation of Supramolecular Hydrogel. *J. Phys. Chem. C* **2009,** *113* (31), 13651-13657.
22. Xu, Y.; Sheng, K.; Li, C.; Shi, G., Self-Assembled Graphene Hydrogel Via a One-Step Hydrothermal Process. *ACS Nano* **2010,** *4* (7), 4324-4330.
23. Simões, S. M. N.; Veiga, F.; Torres-Labandeira, J. J.; Ribeiro, A. C. F.; Sandez-Macho, M. I.; Concheiro, A.; Alvarez-Lorenzo, C., Syringeable Pluronic-A-Cyclodextrin Supramolecular Gels for Sustained Delivery of Vancomycin. *Eur. J. Pharm. Biopharm.* **2012,** *80* (1), 103-112.
24. Harada, A.; Li, J.; Kamachi, M., Double-Stranded Inclusion Complexes of Cyclodextrin Threaded on Poly(Ethylene Glycol). *Nature* **1994,** *370* (6485), 126-128.

25. Liao, X.; Chen, G.; Liu, X.; Chen, W.; Chen, F.; Jiang, M., Photoresponsive Pseudopolyrotaxane Hydrogels Based on Competition of Host-Guest Interactions. *Angew. Chem., Int. Ed.* **2010,** *49* (26), 4409-4413.
26. Ni, X.; Cheng, A.; Li, J., Supramolecular Hydrogels Based on Self-Assembly between Peo-Ppo-Peo Triblock Copolymers and A-Cyclodextrin. *J. Biomed. Mater. Res., Part A* **2009,** *88* (4), 1031-1036.
27. Guo, C. G.; Wang, L.; Li, Y. K.; Wang, C. Q., Suprarmolecular Hydrogels Based on Low-Molecular-Weight Poly(Ethylene Glycol) and A-Cyclodextrin. *J. Appl. Polym. Sci.* **2013,** *129* (2), 901-907.
28. Kataoka, T.; Kidowaki, M.; Zhao, C.; Minamikawa, H.; Shimizu, T.; Ito, K., Local and Network Structure of Thermoreversible Polyrotaxane Hydrogels Based on Poly(Ethylene Glycol) and Methylated A-Cyclodextrins. *J. Phys. Chem. B* **2006,** *110* (48), 24377-24383.
29. Huh, K. M.; Ooya, T.; Lee, W. K.; Sasaki, S.; Kwon, I. C.; Jeong, S. Y.; Yui, N., Supramolecular-Structured Hydrogels Showing a Reversible Phase Transition by Inclusion Complexation between Poly(Ethylene Glycol) Grafted Dextran and A-Cyclodextrin. *Macromolecules* **2001,** *34* (25), 8657-8662.
30. Hoare, T. R.; Kohane, D. S., Hydrogels in Drug Delivery: Progress and Challenges. *Polymer* **2008,** *49* (8), 1993-2007.
31. Fenyvesi, E.; Gruiz, K.; Verstichel, S.; De Wilde, B.; Leitgib, L.; Csabai, K.; Szaniszlo, N., Biodegradation of Cyclodextrins in Soil. *Chemosphere* **2005,** *60* (8), 1001-1008.
32. Nava-Ortíz, C. A. B.; Alvarez-Lorenzo, C.; Bucio, E.; Concheiro, A.; Burillo, G., Cyclodextrin-Functionalized Polyethylene and Polypropylene as Biocompatible Materials for Diclofenac Delivery. *Int. J. Pharm.* **2009,** *382* (1–2), 183-191.
33. Lakkakula, J. R.; Maçedo Krause, R. W., A Vision for Cyclodextrin Nanoparticles in Drug Delivery Systems and Pharmaceutical Applications. *Nanomedicine* **2014,** *9* (6), 877-894.
34. Li, J.; Loh, X. J., Cyclodextrin-Based Supramolecular Architectures: Syntheses, Structures, and Applications for Drug and Gene Delivery. *Adv. Drug Delivery Rev.* **2008,** *60* (9), 1000-1017.
35. Bromberg, L. E.; Ron, E. S., Temperature-Responsive Gels and Thermogelling Polymer Matrices for Protein and Peptide Delivery. *Adv. Drug Delivery Rev.* **1998,** *31* (3), 197-221.
36. Osman, S. K.; Soliman, G. M.; Amin, M.; Zaky, A., Self-Assembling Hydrogels Based on B-Cyclodextrin Polymer and Poly (Ethylene Glycol) Bearing Hydrophobic Moieties for Protein Delivery. *Int. J. Pharm. Pharm. Sci.* **2014,** *6* (7), 591-597.
37. Ma, X.; Zhou, N.; Zhang, T.; Guo, Z.; Hu, W.; Zhu, C.; Ma, D.; Gu, N., In Situ Formation of Multiple Stimuli-Responsive Poly[(Methyl Vinyl Ether)-Alt-(Maleic Acid)]-Based Supramolecular Hydrogels by Inclusion Complexation between Cyclodextrin and Azobenzene. *RSC Advances* **2016,** *6* (16), 13129-13136.
38. Weissleder, R., A Clearer Vision for in Vivo Imaging: Progress Continues in the Development of Smaller, More Penetrable Probes for Biological Imaging. *Nat. Biotechnol.* **2001,** *19* (4), 316-317.
39. Wu, M. C.; Deokar, A. R.; Liao, J. H.; Shih, P. Y.; Ling, Y. C., Graphene-Based Photothermal Agent for Rapid and Effective Killing of Bacteria. *ACS Nano* **2013,** *7* (2), 1281-1290.
40. Robinson, J. T.; Tabakman, S. M.; Liang, Y.; Wang, H.; Sanchez Casalongue, H.; Vinh, D.; Dai, H., Ultrasmall Reduced Graphene Oxide with High near-Infrared Absorbance for Photothermal Therapy. *J. Am. Chem. Soc.* **2011,** *133* (17), 6825-6831.

41. Quinn, M. D. J.; Du, J.; Boyd, B. J.; Hawley, A.; Notley, S. M., Lipid Liquid-Crystal Phase Change Induced through near-Infrared Irradiation of Entrained Graphene Particles. *Langmuir* **2015,** *31* (24), 6605-6609.
42. Wang, T.; Quinn, M. D. J.; Nguyen, S. H. T.; Yu, A.; Notley, S. M., Graphene Films Using a Thermally Curable Surfactant. *Adv. Mater. Interfaces* **2016,** *3* (15).
43. Kogan, A.; Garti, N., Microemulsions as Transdermal Drug Delivery Vehicles. *Adv. Colloid Interface Sci.* **2006,** *123-126* (SPEC. ISS.), 369-385.
44. Batrakova, E. V.; Kabanov, A. V., Pluronic Block Copolymers: Evolution of Drug Delivery Concept from Inert Nanocarriers to Biological Response Modifiers. *J. Controlled Release* **2008,** *130* (2), 98-106.
45. Jokerst, J. V.; Lobovkina, T.; Zare, R. N.; Gambhir, S. S., Nanoparticle Pegylation for Imaging and Therapy. *Nanomedicine* **2011,** *6* (4), 715-728.
46. Paton, K. R.; Coleman, J. N., Relating the Optical Absorption Coefficient of Nanosheet Dispersions to the Intrinsic Monolayer Absorption. *Carbon* **2016,** *107*, 733-738.
47. Wang, T.; Quinn, M. D. J.; Notley, S., A Benzoxazine Surfactant Exchange for Atomic Force Microscopy Characterization of Two Dimensional Materials Exfoliated in Aqueous Surfactant Solutions. *RSC Advances* **2017,** *7* (6), 3222-3228.
48. Dan, L.; Müller, M. B.; Gilje, S.; Kaner, R. B.; Wallace, G. G., Processable Aqueous Dispersions of Graphene Nanosheets. *Nat. Nanotechnol.* **2008,** *3* (2), 101-105.
49. Paton, K. R.; Varrla, E.; Backes, C.; Smith, R. J.; Khan, U.; O'Neill, A.; Boland, C.; Lotya, M.; Istrate, O. M.; King, P.; Higgins, T.; Barwich, S.; May, P.; Puczkarski, P.; Ahmed, I.; Moebius, M.; Pettersson, H.; Long, E.; Coelho, J.; O'Brien, S. E.; McGuire, E. K.; Sanchez, B. M.; Duesberg, G. S.; McEvoy, N.; Pennycook, T. J.; Downing, C.; Crossley, A.; Nicolosi, V.; Coleman, J. N., Scalable Production of Large Quantities of Defect-Free Few-Layer Graphene by Shear Exfoliation in Liquids. *Nat. Mater.* **2014,** *13* (6), 624-630.
50. Kang, M. S.; Kim, K. T.; Lee, J. U.; Jo, W. H., Direct Exfoliation of Graphite Using a Non-Ionic Polymer Surfactant for Fabrication of Transparent and Conductive Graphene Films. *J. Mater. Chem. C* **2013,** *1* (9), 1870-1875.
51. Ferrari, A. C.; Basko, D. M., Raman Spectroscopy as a Versatile Tool for Studying the Properties of Graphene. *Nat. Nanotechnol.* **2013,** *8* (4), 235-246.
52. Lotya, M.; Rakovich, A.; Donegan, J. F.; Coleman, J. N., Measuring the Lateral Size of Liquid-Exfoliated Nanosheets with Dynamic Light Scattering. *Nanotechnology* **2013,** *24* (26).
53. Coleman, J. N., Liquid Exfoliation of Defect-Free Graphene. *Acc. Chem. Res.* **2013,** *46* (1), 14-22.
54. Moussa, S.; Atkinson, G.; Samyel-Shall, M.; Shehata, A.; Abouzeid, K. M.; Mohamed, M. B., Laser Assisted Photocatalytic Reduction of Metal Ions by Graphene Oxide. *J. Mater. Chem.* **2011,** *21* (26), 9608-9619.
55. Abdelsayed, V.; Moussa, S.; Hassan, H. M.; Aluri, H. S.; Collinson, M. M.; El-Shall, M. S., Photothermal Deoxygenation of Graphite Oxide with Laser Excitation in Solution and Graphene-Aided Increase in Water Temperature. *J. Phys. Chem. Lett.* **2010,** *1* (19), 2804-2809.
56. Balandin, A. A.; Ghosh, S.; Bao, W.; Calizo, I.; Teweldebrhan, D.; Miao, F.; Lau, C. N., Superior Thermal Conductivity of Single-Layer Graphene. *Nano Lett.* **2008,** *8* (3), 902-907.
57. Lotya, M.; Hernandez, Y.; King, P. J.; Smith, R. J.; Nicolosi, V.; Karlsson, L. S.; Blighe, F. M.; De, S.; Zhiming, W.; McGovern, I. T.; Duesberg, G. S.; Coleman, J. N., Liquid Phase Production of Graphene by Exfoliation of Graphite in Surfactant/Water Solutions. *J. Am. Chem. Soc.* **2009,** *131* (10), 3611-3620.

58. Kapitza, P. L., Heat Transfer and Superfluidity of Helium Ii. *Physical Review* **1941,** *60* (4), 354-355.
59. Alexeev, D.; Chen, J.; Walther, J. H.; Giapis, K. P.; Angelikopoulos, P.; Koumoutsakos, P., Kapitza Resistance between Few-Layer Graphene and Water: Liquid Layering Effects. *Nano Lett.* **2015,** *15* (9), 5744-5749.
60. Swartz, E. T.; Pohl, R. O., Thermal Boundary Resistance. *Rev. Mod. Phys.* **1989,** *61* (3), 605-668.
61. Philip, J.; Shima, P. D.; Raj, B., Enhancement of Thermal Conductivity in Magnetite Based Nanofluid Due to Chainlike Structures. *Appl. Phys. Lett.* **2007,** *91* (20), 203108.
62. Prasher, R.; Phelan, P. E.; Bhattacharya, P., Effect of Aggregation Kinetics on the Thermal Conductivity of Nanoscale Colloidal Solutions (Nanofluid). *Nano Lett.* **2006,** *6* (7), 1529-1534.
63. Keblinski, P.; Phillpot, S. R.; Choi, S. U. S.; Eastman, J. A., Mechanisms of Heat Flow in Suspensions of Nano-Sized Particles (Nanofluids). *Int. J. Heat Mass Transfer* **2002,** *45* (4), 855-863.
64. Ye, L.; Liu, J.; Sheng, P.; Huang, J. S.; Weitz, D. A., Sound Propagation in Colloidal Systems. *Journal De Physique. IV : JP* **1993,** *3* (1), 183-196.
65. Angayarkanni, S. A.; Philip, J., Review on Thermal Properties of Nanofluids: Recent Developments. *Adv. Colloid Interface Sci.* **2015,** *225*, 146-176.
66. Cvetkovic, A.; Picioreanu, C.; Straathof, A. J. J.; Krishna, R.; Van Der Wielen, L. A. M., Relation between Pore Sizes of Protein Crystals and Anisotropic Solute Diffusivities. *J. Am. Chem. Soc.* **2005,** *127* (3), 875-879.
67. Zhu, W.; Li, Y.; Liu, L.; Chen, Y.; Wang, C.; Xi, F., Supramolecular Hydrogels from Cisplatin-Loaded Block Copolymer Nanoparticles and A-Cyclodextrins with a Stepwise Delivery Property. *Biomacromolecules* **2010,** *11* (11), 3086-3092.
68. Arunan, E.; Desiraju, G. R.; Klein, R. A.; Sadlej, J.; Scheiner, S.; Alkorta, I.; Clary, D. C.; Crabtree, R. H.; Dannenberg, J. J.; Hobza, P.; Kjaergaard, H. G.; Legon, A. C.; Mennucci, B.; Nesbitt, D. J., Defining the Hydrogen Bond: An Account (Iupac Technical Report). *Pure Appl. Chem.* **2011,** *83* (8), 1619-1636.
69. Yu, L.; Zhang, H.; Ding, J., A Subtle End-Group Effect on Macroscopic Physical Gelation of Triblock Copolymer Aqueous Solutions. *Angew. Chem., Int. Ed.* **2006,** *45* (14), 2232-2235.
70. Xue, R.; Xin, X.; Wang, L.; Shen, J.; Ji, F.; Li, W.; Jia, C.; Xu, G., A Systematic Study of the Effect of Molecular Weights of Polyvinyl Alcohol on Polyvinyl Alcohol-Graphene Oxide Composite Hydrogels. *Phys. Chem. Chem. Phys.* **2015,** *17* (7), 5431-5440.

Table of Contents Graphic

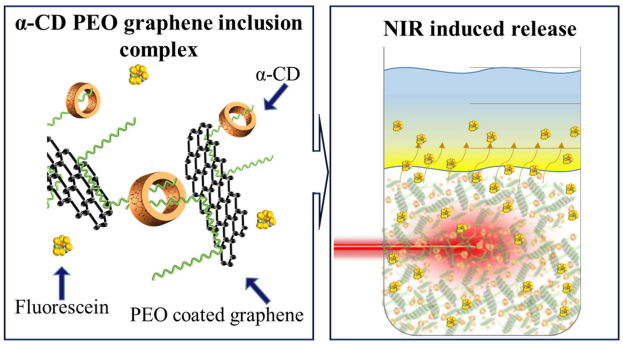

Highlights

- Successful incorporation of surfactant exfoliated graphene as an intrinsic component (not an additive) of an alpha-cyclodextrin based gel.
- Exploration of gelation properties of the hybrid gels and the relationship with PEO composition.
- Demonstration of photothermally induced drug release through near-infrared irradiation of embedded graphene
- Extensive characterisation of the gels produced with a focus on the drug release properties.